Nanoscale

PAPER

Cite this: *Nanoscale*, 2019, **11**, 20589

Optothermal microbubble assisted manufacturing of nanogap-rich structures for active chemical sensing†

Farzia Karim, [a] Erick S. Vasquez, [b] Yvonne Sun[c] and Chenglong Zhao *[a,d]

Received 11th July 2019,
Accepted 2nd October 2019

DOI: 10.1039/c9nr05892c

rsc.li/nanoscale

Guiding analytes to the sensing area is an indispensable step in a sensing system. Most of the sensing systems apply a passive sensing method, which waits for the analytes to diffuse towards the sensor. However, passive sensing methods limit the detection of analytes to a picomolar range on micro/nano-sensors for a practical time scale. Therefore, active sensing methods need to be used to improve the detection limit in which the analytes are forced to concentrate on the sensors. In this article, we have demonstrated the manufacturing of nanogap-rich structures for active chemical sensing. Nanogap-rich structures are manufactured from metallic nanoparticles through an optothermally generated microbubble (OGMB) which is a laser-induced micron-sized bubble. The OGMB induces a strong convective flow that helps to deposit metallic nanoparticles to form nanogap-rich structures on a solid surface. In addition, the OGMB is used to guide and concentrate analytes towards the nanogap-rich structures for the active sensing of analytes. An active sensing method can improve the detection limit of chemical substances by an order of magnitude compared to a passive sensing method. The microbubble assisted manufacturing of nanogap-rich structures together with an active analyte sensing method paves a new way for advanced chemical and bio-sensing applications.

Introduction

The evaluation of a chemical sensing system depends on two key parameters namely detection sensitivity and time. These are two important however contradictory parameters among other parameters in a sensing system. The signal-to-noise ratio of a sensor increases with the decreasing size of the active sensing area, which helps ultrasensitive sensing at extremely low concentrations. However, a smaller sensing area also means that the analytes will take longer time to diffuse towards the sensor to generate an effective sensing signal, especially when the analytes are in a highly diluted solution.[1,2] For instance, theoretical calculations have shown that it takes around one hour for the first analyte to bind to a micro-sensor when the concentration of analytes is one femtomolar. It can even take several days if the size of the sensor is on the nanoscale.[2]

The impractical long waiting time is a result of the passive sensing method that is used in most of the sensing systems, where the binding takes place after waiting for the analytes to freely diffuse towards the sensor surface. This passive sensing method works when the analytes are at high concentrations because the chances of analytes to interact with the sensor are higher. However, the passive sensing method fails to work when the analytes are in a highly diluted solution because the analytes spend unrealistically long times to diffuse towards the small sensing area, or in other words, this is a diffusion-limited method.[3–6] Sheehan *et al.* have predicted that "individual nanoscale sensors will be limited to picomolar-order sensitivity for practical time scales".[2]

To overcome the diffusion limit, active sensing can be applied to force the analytes towards the sensor. Therefore, it can significantly reduce the waiting time for an effective analyte-sensor binding and thereby improve the detection limit by locally increasing the concentration of analytes. Several active sensing methods have been demonstrated in the literature. For example, a superhydrophobic artificial surface combined with an evaporating liquid droplet has been demonstrated to break the diffusion limit.[5] The droplet containing analytes can slide on the superhydrophobic surface as it evap-

[a]*Department of Electro-Optics and Photonics, University of Dayton, 300 College Park, Dayton, OH 45469, USA*
[b]*Department of Chemical and Materials Engineering, University of Dayton, 300 College Park, Dayton, OH 45469, USA*
[c]*Department of Biology, University of Dayton, 300 College Park, Dayton, OH 45469, USA*
[d]*Department of Physics, University of Dayton, 300 College Park, Dayton, OH 45469, USA. E-mail: czhao1@udayton.edu*

†Electronic supplementary information (ESI) available. See DOI: 10.1039/c9nr05892c

orates without being pinned at its initial contact point.[7–10] The recognition and localization of a single lambda DNA molecule have been successfully demonstrated using this system. A slippery substrate that allows for the free movement of a droplet on a substrate to achieve similar functions is also demonstrated by Yang *et al.*[11] However, these methods require the preparation of a superhydrophobic substrate with artificially designed nanostructures, which typically involves an expensive nanofabrication process and also limits the type of substrate that can be used in the sensing process.

Another effort to actively control the localization of analytes is achieved by forcing the analytes to flow through nanochannels with an external electric field.[12,13] An array of nanoholes in a gold film is integrated with a microfluidic system to serve as both a plasmonic sensor and flow-through nanochannels. Voltage is applied across the solution to force the analytes to concentrate on the sensor. However, this method is only applicable to the sensors consisting of nanoholes and the liquid solution needs to be specially modified to work under an electric field.

In addition to these efforts, nano-sensors consisting of free-moving nanoparticles with surface modifications can be used to target the analytes to increase the binding rate.[14–18] However, the problem of the diffusion limit is still not solved in this case because the nano-sensor together with the analytes must diffuse to a small exciting light source to create an effective detection. Recently, another active sensing method is demonstrated by Garcia-Guirado *et al.* based on an electrothermoplasmonic effect on a localized surface plasmon resonance (LSPR) sensing chip.[19]

Micro/nano-sensors consisting of nanogap-rich structures are one important category of sensors which have been widely used for surface enhanced Raman scattering (SERS). For example, Liu *et al.* have fabricated gold nanosphere arrays with rich nanogaps by using a self-assembly process.[20–22] The large electromagnetic field in the nanogaps leads to large SERS enhancement and enables a wide range of applications such as sensing, catalysis and biology.[21,22] Another nanogap-rich structure has been fabricated through the chemical synthesis of aluminum nanocrystals and used for SERS based DNA detection.[23] Yang *et al.* have fabricated Ag nanoplate arrays for SERS biosensing applications through electrodeposition and an *in situ* electro-corrosion method.[24] Several other structures such as 3D Ag@ZnO nanostructures,[25] porous silicon nanopillar arrays,[26] split wedge antennas,[27] and Ag ring arrays[28] have been fabricated for SERS based sensing. However, most of these sensors still rely on passive sensing, *i.e.* waiting for the analytes to diffuse towards the sensors. Therefore, these are still diffusion limited.

In this work, a microbubble assisted manufacturing method is demonstrated which allows us not only to rapidly fabricate nanogap-rich structures under ambient conditions, but also to actively guide and concentrate analytes to the nanogap-rich structures for the active sensing of analytes. The active sensing method works based on an optothermally generated microbubble (OGMB), which is a micron-sized bubble that is formed on a liquid–solid interface by laser heating. The position and size of an OGMB can be remotely controlled by the laser. The OGMB induces a strong Marangoni convective flow[29–34] around it which can be used for many applications including particle trapping,[30] plasmofluidic lenses,[35] photothermal motors,[36] fabrication of pattern structures,[37–40] and microfluidic applications.[41] More details about the OGMB can be found in a review article by Xie *et al.*[33] Recently, OGMB based chemical sensing[28] and biosensing[42] have been demonstrated. This work differs from the work presented in refs. 28 and 42 as follows: the OGMB is used not only to fabricate SERS substrates under ambient conditions but also to concentrate analytes for active sensing. The Rhodamine 6G (R6G) molecule and Malachite Green (MG) fungicide can be detected at a concentration as low as 10 femtomolar. The active sensing method can improve the detection limit of analytes by an order of magnitude compared to a passive sensing method.

Results and discussion

Fabrication of nanogap-rich structures through an OGMB

Fig. 1a schematically shows the working principle of OGMB assisted manufacturing of nanogap-rich structures for the active sensing of analytes. A detailed working flow can be found in Fig. S1.† Briefly, a nanogap-rich structure consisting of gold nanoparticles is first fabricated at a solid–liquid interface through an OGMB. The OGMB is generated by laser heating and induces a strong Marangoni convective flow around it which helps to rapidly deposit nanoparticles to form nanogap-rich structures on a substrate [Fig. S1 and Movie S1†]. The Marangoni convective flow around the OGMB also guides and concentrates analytes on the nanogap-rich structure for active sensing. It should be noted that nanogap-rich structures are used here solely for the proof of concept. The active sensing method demonstrated in this article is also applicable to other types of sensing platforms.

Nanogap-rich structures consisting of two types of nanoparticles (gold nanospheres and gold nanoshells) are fabricated on a gold-coated glass substrate by using an OGMB through the same procedure as described in our previous work.[43] Briefly, a droplet of gold nanosphere (or nanoshells) solution is placed on a gold-coated glass substrate. An OGMB is generated inside the droplet by focusing a laser on the gold-coated glass substrate [Fig. S1†]. The OGMB induces a strong convective flow around it, which helps to deposit nanospheres (or nanoshells) on the gold-coated-glass substrate [Movie S1†] to form nanogap-rich structures. Gold nanospheres have a diameter of 200 nm as shown in the TEM image of Fig. 1d which were purchased from BBI Solution. Gold nanoshells (silica core) with a diameter of 240 nm consist of a 200 nm silica core coated with 20 nm gold nanospheres as depicted in the TEM image of Fig. 1g which were purchased from NanoComposix. Nanogap-rich structures fabricated from gold nanospheres and gold nanoshells (silica core) are referred in this work as gold-nanosphere-structures and gold-nanoshell-structures, respectively. The optical images of a gold-nanosphere-structure

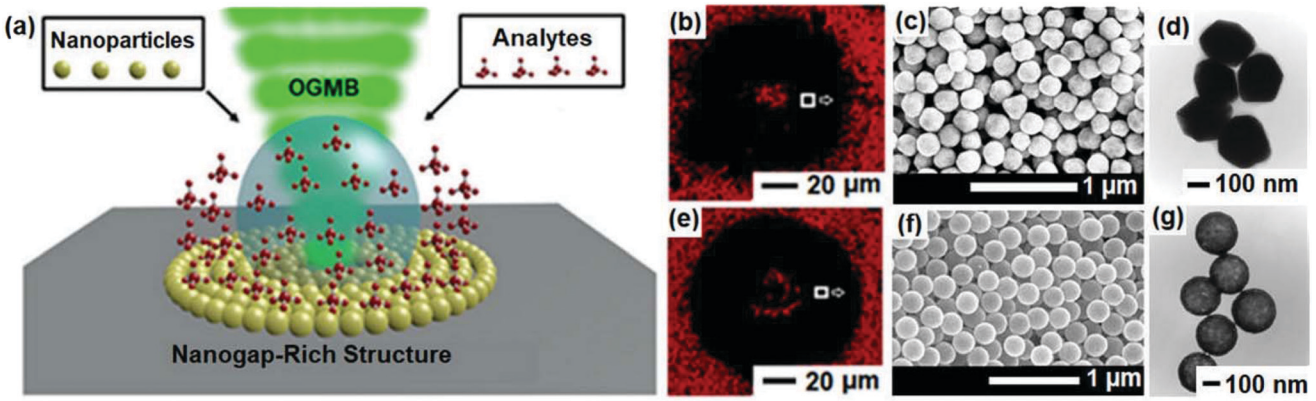

Fig. 1 (a) Schematic of the active sensing by a nanogap-rich structure with an OGMB. (b) Optical image of a nanogap rich structure fabricated from gold nanospheres (gold-nanosphere-structure). (c) SEM image of the corresponding area indicated in (b) by a white box. (d) TEM image of 200 nm gold-nanospheres used to fabricate the gold-nanosphere-structure (e) Optical image of a nanogap-rich structure fabricated from gold nanoshells (gold-nanoshell-structure). (f) SEM image of the corresponding area indicated in (e) by a white box. (g) TEM image of 240 nm gold-nanoshells (200 nm silica core coated with 20 nm gold nanospheres) used to fabricate the gold-nanoshell-structure.

and a gold-nanoshell-structure are shown in Fig. 1b and e, respectively. These are ring-shaped structures with diameters of (97 ± 1) μm and (102 ± 1) μm, respectively. Fig. 1c and f illustrate the scanning electron microscopy (SEM) images of two nanogap-rich structures corresponding to the areas marked by a white box in Fig. 1b and e, respectively. Gold nanospheres and gold nanoshells in the nanogap-rich structures form many nanogaps that are ideal for SERS enhancement due to the plasmonic resonance.[44–46] Nanogap-rich structures fabricated through the OGMB are stable even after 10 minutes of sonication in DI water [Fig. S2†].

Performance of gold-nanosphere-structures

Passive sensing. First, the performance of the gold-nanosphere-structure fabricated from gold-nanospheres is tested by recording the SERS spectra of Rhodamine 6G (R6G) molecules at different concentrations with passive sensing as shown in Fig. 2a. Under these passive sensing conditions, R6G molecules are let freely diffuse to the nanosphere structure and the SERS spectra of R6G are obtained on the nanosphere structure by using a Raman spectrometer (Renishaw inVia Reflex Micro-Raman). We refer this procedure as passive sensing as schematically shown in the inset of Fig. 2b. A laser with a wavelength of 785 nm and a power of 30 mW is focused on the gold-nanosphere structures to record the SERS spectra of R6G. An acquisition time of 10 seconds is used in the data acquisition.

The following characteristic Raman peaks of R6G are clearly shown which closely correspond to the Raman peaks of R6G as reported in the literature:[47,48] C–C stretching (1364 cm^{-1}, 1510 cm^{-1}, 1651 cm^{-1}), N–H in-plane bending (1310 cm^{-1}, 1575 cm^{-1}), C–H in-plane bending (1130 cm^{-1}, 1183 cm^{-1}), C–H out-of-plane bending (775 cm^{-1}), and C–C–C ring in-plane vibration (613 cm^{-1}). Fig. 2b shows the SERS spectra of R6G at lower concentrations. The intensity of the SERS signal decreases with the decreasing R6G concentrations. R6G is detectable at a concentration of 10 pM on the gold-nanosphere-structure with passive sensing as shown in Fig. 2b. The gold-nanosphere-structure gives an average SERS enhancement factor (EF) of 1.2×10^6 [Fig. S3(a)†].

Active sensing. Here, active sensing means actively guiding and concentrating the analytes towards a sensor. For example, Fig. S4† shows the accumulation of R6G molecules on a gold film by applying this active sensing method. An OGMB is generated on a gold film inside a droplet of R6G solution as schematically shown in Fig. S4(a).† Due to Marangoni convective flow associated with the OGMB, R6G molecules are successfully guided and concentrated on the gold film where the OGMB is located as shown in Fig. S4(b).†

To test the performance of the gold-nanosphere-structure under active sensing, an OGMB is generated on the gold-nanosphere-structure from R6G solution as schematically shown in the inset of Fig. 2d. Because of strong convective flow induced by the OGMB, R6G molecules are guided and concentrated on the surface of the gold-nanosphere-structure in the same way as they concentrated on the gold film [Fig. S4(b)†]. Once R6G molecules are concentrated on the surface of the gold-nanosphere-structure, the SERS spectra of R6G molecules at different concentrations are recorded. SERS spectra for active sensing are collected under the following similar experimental conditions of passive sensing: 785 nm laser wavelength, 30 mW laser power, and 10 second acquisition time. Fig. 2c shows the SERS spectra of R6G molecules at different concentrations after applying the active sensing method. Fig. 2d shows the SERS spectra of R6G at lower concentrations. R6G can be successfully detected at a concentration of 1 pM by applying the active sensing method. In contrast, it is not detectable on the same gold-nanosphere-structure by the passive sensing method. Fig. 2e shows the normalized SERS intensity of R6G at 1364 cm^{-1} through passive sensing (dashed line) and active sensing (solid line) as a function of the R6G concentration. Experimental error bars of SERS intensity at 1364 cm^{-1} for all the concentrations of R6G for both active

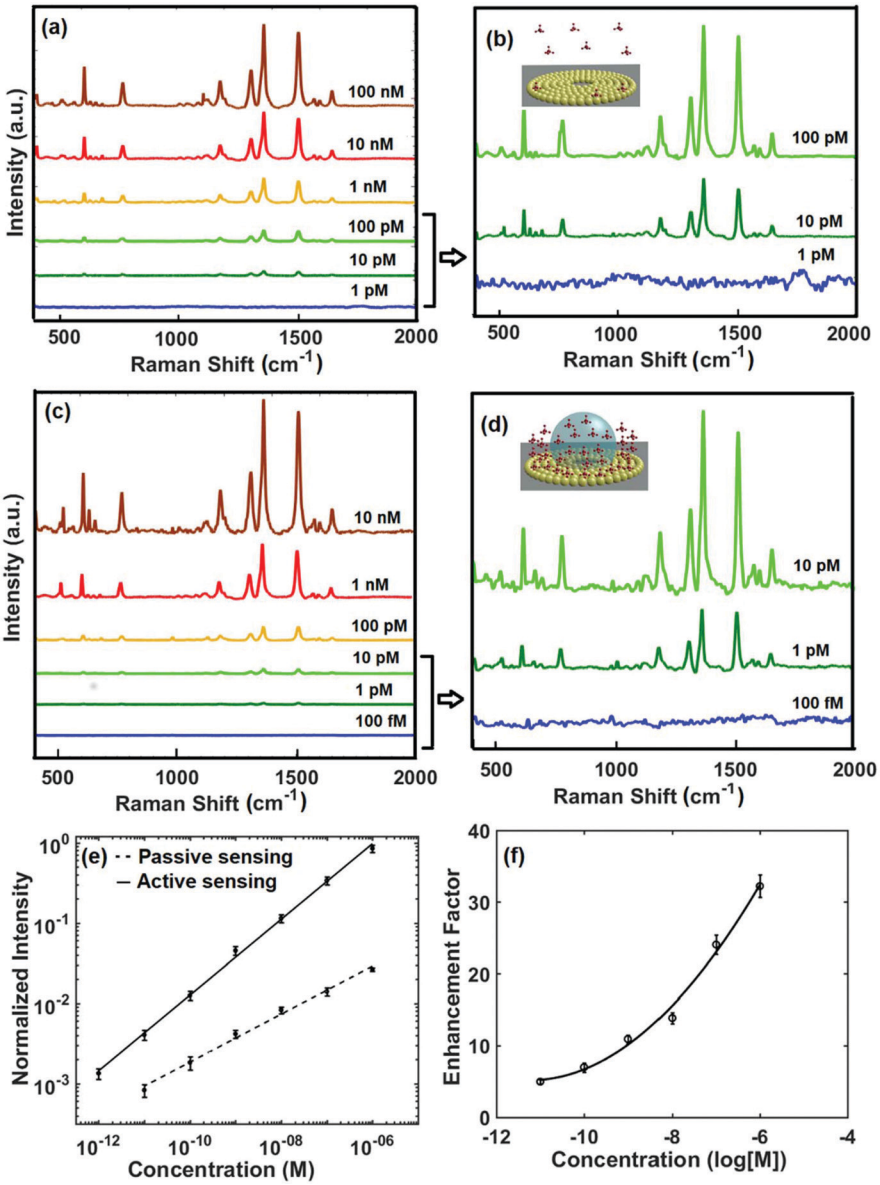

Fig. 2 (a) SERS spectra of R6G at different concentrations (100 nM to 1 pM) collected from gold-nanosphere-structures with the passive sensing method. (b) Magnified spectra at lower concentrations (100 pM to 1 pM) marked in (a) by an arrow. Inset: schematic of passive sensing methods. (c) SERS spectra of R6G at different concentrations (10 nM to 100 fM) collected from the gold-nanosphere-structure by the active sensing method. (d) Magnified spectra at lower concentrations (10 pM to 100 fM) marked in (c) by an arrow. Inset: schematic of the active sensing method. (e) Normalized SERS intensity of R6G at 1364 cm^{-1} as a function of the R6G concentration through active sensing (solid line) and passive sensing (dashed line) methods with error bars indicating the experimental standard deviations. (f) Enhancement factor of the gold-nanosphere-structure as a function of R6G concentrations because of active sensing.

sensing and passive sensing are calculated from four sets of SERS spectra recorded at four different spots of the gold-nanosphere-structure. The experimental data are well fitted with the following functions: active sensing, $\log_{10}(y) = 0.47 \log_{10}(x) + 2.82$ with $R^2 = 0.998$ and passive sensing, $\log_{10}(y) = 0.30 \log_{10}(x) + 0.26$ with $R^2 = 0.994$. Here, x represents the concentration of R6G, and y represents the normalized SERS intensity of R6G at 1364 cm^{-1}. The gold-nanosphere-structure achieves higher sensitivity by active sensing than by passive sensing.

Besides the SERS enhancement of the Raman signal, active sensing can give rise to an additional enhancement factor due to the analyte concentration. It should be noted that the enhancement due to the analyte concentration is different from the SERS enhancement. The SERS enhancement is a result of the enhanced electric field in the nanogaps of the gold-nanosphere-structure. In contrast, the enhancement due to the analyte concentration is a result of the OGMB based analyte concentration. The enhancement factor due to the analyte concentration is calculated as the ratio of the Raman

peak of R6G at 1364 cm^{-1} for active sensing (Fig. 2c) to that for passive sensing (Fig. 2a) at the same concentration. Fig. 2f shows the enhancement factor due to the analyte concentration as a function of the R6G concentration for the gold-nanosphere-structure. The experimental data are fitted with the equation $y = 0.99x + 22.33x + 130.59$ with $R^2 = 0.991$. Here, x represents the log of concentration of R6G and y represents the enhancement factor due to the analyte concentration. Besides the SERS enhancement factor of 1.2×10^6 achieved on the gold-nanosphere-structure, the additional enhancement factors due to the analyte concentrations of around 5 ± 0.3 and 32 ± 1.5 are achieved at a concentration of 10 pM and 1 μM, respectively. A higher concentration of analytes results in a higher enhancement because the molecules have a larger probability to be captured and concentrated on the surface of the nanogap-rich structure due to the convective flow induced by the OGMB.

Performance of the gold-nanoshell-structure

The gold-nanosphere-structure can achieve a detection limit of 1 pM by applying the active sensing method. This detection limit can be further improved by using a gold-nanoshell-structure. The gold-nanoshell-structure is fabricated on a gold-coated glass substrate as shown in Fig. 1e and f. Fig. 3a shows the SERS spectra of R6G at different concentrations obtained by the passive sensing method, *i.e.* letting R6G molecules freely diffuse to the gold-nanoshell-structure. Fig. 3b shows the same SERS spectra at lower concentrations. A detection limit of 100 fM is achieved with the gold-nanoshell-structure, indicating an improvement of the detection limit as compared to the gold-nanosphere-structure. Fig. 3c shows the SERS spectra of R6G molecules at different concentrations by the active sensing method, *i.e.* generating an OGMB on the gold-nanoshell-structure to actively guide and concentrate R6G on the gold-nanoshell-structure. Fig. 3d shows the SERS spectra at lower concentrations. The active sensing method can push the detection limit to 10 fM concentration of R6G. The same experimental parameters (laser wavelength of 785 nm, laser power of 30 mW and exposure time of 10 seconds) which are used in the case of the gold-nanosphere-structure are also used to obtain the SERS spectra of R6G collected from the gold-nanoshell-structure. The average SERS enhancement factor (EF) of the gold-nanoshell-structure is 1.1×10^7 [Fig. S3(b)†], which is an order of magnitude higher than that of the gold-nanosphere-structure. Fig. 3e shows the normalized SERS intensity of R6G at 1364 cm^{-1} with passive sensing (dashed line) and active sensing (solid line), respectively, as a function of the R6G concentration. The experimental data are a good fit with the following functions: active sensing, $\log_{10}(y) = 0.42 \log_{10}(x) + 2.46$ with $R^2 = 0.998$ and passive sensing, $\log_{10}(y) = 0.29 \log_{10}(x) + 0.08$ with $R^2 = 0.999$. Here, x represents the concentration of R6G, and y is the normalized SERS intensity of R6G at 1364 cm^{-1}.

The additional enhancement factor of the gold-nanoshell-structure due to the analyte concentration as a function of the R6G concentration is plotted in Fig. 3f. The experimental data are fitted with the function of $y = 0.72x^2 + 19.02x + 130.58$ with $R^2 = 0.995$. Here, x is the log of concentration of R6G and y is the enhancement factor of the gold-nanoshell-structure due to the analyte concentration. An enhancement factor due to the analyte concentration of 5 ± 0.6 is achieved even at a concentration of 100 fM. It should be noted that the enhancement factor due to the analyte concentration not only depends on the concentration of analytes but also depends on the type of nanogap-rich-structure. For example, the enhancement factor of 1 μM R6G on a gold-nanoshell-structure is 43 ± 1.6. In contrast, the enhancement factor is 32 ± 1.5 on a gold-nanosphere-structure at the same concentration of R6G.

Comparison of two nanogap-rich-structures

Based on the data shown for the two nanogap-rich-structures (gold-nanoshell-structure and gold-nanosphere-structure), the gold-nanoshell-structure has better performance than the gold-nanosphere-structure because of the higher electric field and more hot-spots available on the gold-nanoshell-structure. Fig. 4a and b show the electric field profile of an array of the gold-nanosphere-structure and gold-nanoshell-structure, respectively, which are simulated by the finite-difference-time-domain (FDTD) method. A laser wavelength of 785 nm is used in the simulation, which is the same wavelength used in the experiment to record the SERS spectra of R6G. Here, an array of the gold nanospheres (inset of Fig. 4a) and nanoshells (inset of Fig. 4b) is used in the simulation to mimic the nanogap-rich structures fabricated in the experiment. The maximum electric fields (14 V m^{-1}), or hot-spots, are mainly located between the gold nanospheres for the gold-nanosphere-structure as shown in Fig. 4a. In contrast, the maximum electric fields (57 V m^{-1}) are mainly located on the surface of the gold nanoshells (silica core) for the gold-nanoshell-structure as shown in Fig. 4b. In addition, there are more hot-spots for the gold-nanoshell-structure than for the gold-nanosphere-structure as shown in Fig. 4(b) due to the structure of the gold nanoshell (silica core). Each gold nanoshell (silica core) consists of a 200 nm silica core coated with 20 nm gold-nanospheres. Therefore, the highest electric fields or hot-spots are observed between the gold nanospheres coated on the silica core of the gold-nanoshell. The more hot-spots and higher electric fields on the gold-nanoshell-structure compared to the gold-nanosphere-structure result in a higher Raman signal on the gold-nanoshell-structure because the Raman signal is approximately proportional to the fourth order of the electric field.[49] Fig. 4c shows the SERS spectrum of 1 μM R6G molecules collected from the gold-nanosphere-structure and gold-nanoshell-structure, respectively. The Raman peak of R6G at 1364 cm^{-1} on the gold-nanoshell-structure is around 13 times higher than that on the gold-nanosphere-structure.

In addition, the uniformity of the two nanogap-rich structures (gold-nanosphere-structure and gold-nanoshell-structure) is estimated from the SERS signals collected from 15 different positions of two nanogap-rich structures. The histogram of SERS intensity of 100 pM R6G at 1364 cm^{-1} from the gold-nanosphere-structure and gold-nanoshell-structure is depicted in Fig. 4(d) and (e), respectively. The SERS signals of R6G are

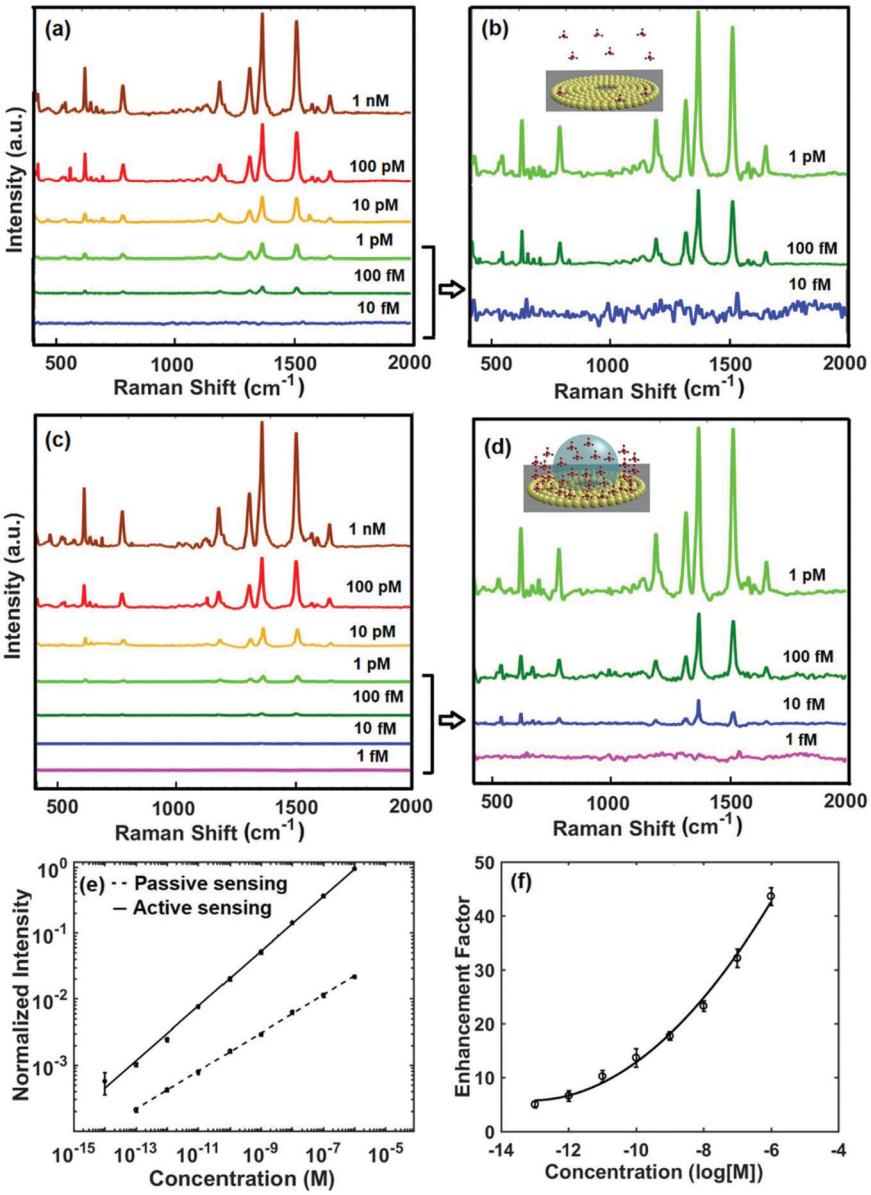

Fig. 3 (a) SERS spectra of R6G with different concentrations (1 nM to 10 fM) collected from the gold-nanoshell-structure by the passive sensing method. (b) Magnified spectra corresponding to lower concentrations (1 pM to 10 fM) of R6G marked in (a) by an arrow. Inset: schematic of passive sensing. (c) SERS spectra of different concentrations (1 nM to 1 fM) of R6G collected from the gold-nanoshell-structure by the active sensing method. (d) Magnified spectra of R6G at lower concentrations (1 pM to 1 fM) indicated in (c) by an arrow. Inset: schematic of active sensing. (e) Normalized SERS intensity of R6G at 1364 cm^{-1} *versus* R6G concentration by active sensing (solid line) and passive sensing (dashed line). (f) Enhancement factor of the gold-nanoshell-structure *versus* R6G concentrations due to active sensing.

recorded from 15 random sites of the gold-nanosphere-structure and gold-nanoshell-structure. The variation of SERS intensity, ΔI, with respect to the average SERS intensity, I_{ave} (the red solid line in Fig. 4d and e), is calculated as follows:

$$\Delta I = \frac{|I_m - I_{ave}|}{I_m} \times 100\% \quad (1)$$

where I_m is the minimum or maximum SERS intensity in the measurement. According to the above formula, the minimum and maximum variations of SERS intensity are 5% and 20% for the gold-nanosphere-structure, respectively. For the gold-nanoshell-structure, the minimum and maximum SERS intensity variations are 3% and 15% respectively. The variation in SERS intensity is a result of different numbers of nanogaps that exist within the Raman exciting laser spot, which is determined by the OGMB-assisted fabrication process. A large variation of SERS intensity is not observed in the experiment, which indicates the good uniformity of the nanogap-rich structures that are fabricated through the OGMB.

In this work, R6G molecules are used to test the active sensing method and are commonly used as a benchmark for

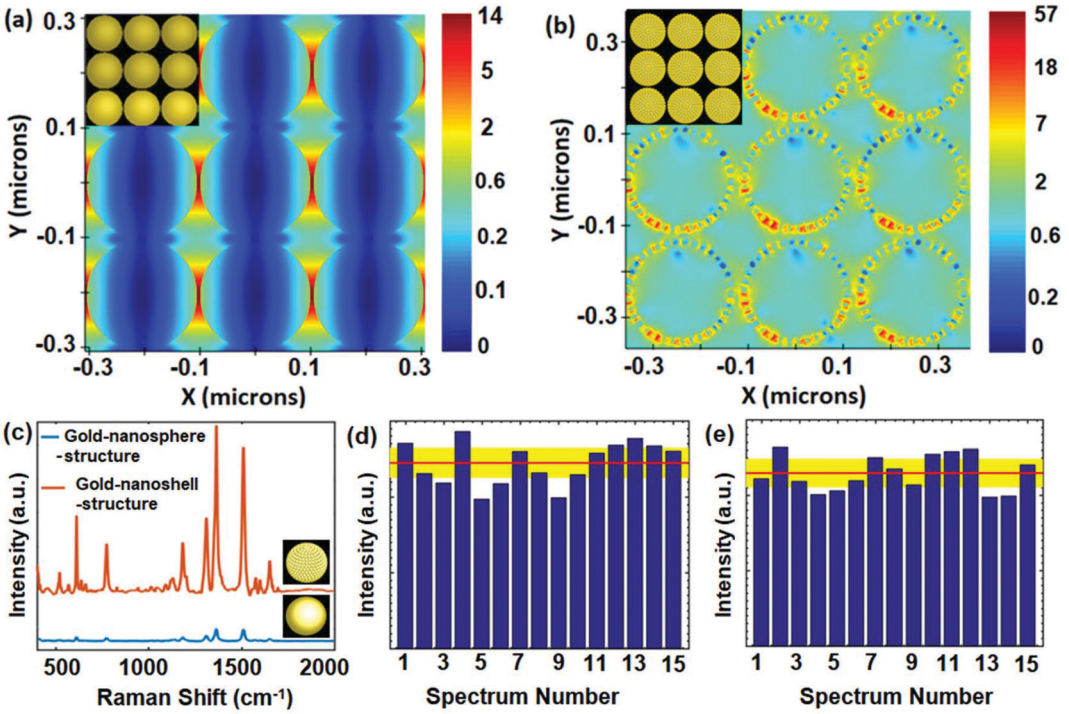

Fig. 4 (a) Electric field profile of the gold nanosphere array at an exciting laser wavelength at 785 nm. Inset: structure of the gold nanosphere array. (b) Electric field profile of the gold nanoshell (silica core) array at 785 nm laser wavelength. Inset: structure of the gold nanoshell (silica core) array. (c) SERS spectrum of 1 μM R6G collected from the gold-nanosphere-structure and gold-nanoshell-structure respectively. (d, e) The histogram of SERS intensity variation of 100 pM R6G at 1364 cm^{-1}. SERS spectra are collected from 15 different positions of (d) a gold-nanosphere-structure and (e) a gold-nanoshell-structure.

Raman spectroscopy.[50,51] We have also tested the active sensing method on a gold-nanoshell-structure through the detection of malachite green (MG) fungicide down to 10 fM concentration [Fig. S5†].

Conclusions

We have demonstrated an active sensing method based on an OGMB. The OGMB is used to fabricate two types of nanogap-rich-structures under ambient conditions: gold-nanosphere-structure and gold-nanoshell-structure. The SERS enhancement factors of 1.2×10^6 and 1.1×10^7 are achieved from the gold-nanosphere-structure and gold-nanoshell-structure, respectively. In addition to the SERS enhancement, active sensing can provide an additional enhancement factor due to the analyte concentration ranging from 5 ± 0.6 to 43 ± 1.6 for the gold-nanoshell-structure depending on the concentration of analytes. A detection limit of 10 fM is achieved for the detection of R6G and MG molecules on the gold-nanoshell-structure by the active sensing method. The fabrication of a nanogap-rich structure and active sensing are separated in the current experiment. For example, gold nanoparticles are first deposited on a substrate by using an OGMB to form a nanogap-rich structure. The analyte solution is then concentrated on the nanogap-rich structure with another OGMB for active sensing. However, these two processes can be combined. For example, the gold nanoparticle solution can be premixed with the analyte solution. Then the surface of gold nanoparticles can be modified to bind a specific analyte. An OGMB can be used to deposit nanoparticles and concentrate analytes on the surface. For example, Tantussi *et al.* demonstrated this concept in their most recent article, where they premixed gold nanoparticles with extracellular membrane vehicles (EVs) to concentrate EVs through an OGMB.[42] It should be noted that an OGMB can be generated on other types of sensors for active sensing. Therefore, the active sensing method can be easily adopted in other sensing systems to improve the detection limit and thus pave the way for advanced chemical and biosensing applications.

Materials and methods

Materials

Gold nanospheres with a diameter of 200 nm were purchased from BBI solutions. 240 nm gold nanoshells (200 nm silica core coated with 20 nm gold nanospheres) were purchased from NanoComposix. Rhodamine 6G (R6G) molecules were purchased from Sigma-Aldrich. Malachite Green (MG) Oxalate was purchased from MP Biomedicals. All the chemicals were used in our experiment as received without further purification.

Nanogap-rich structure fabrication

The nanogap-rich structures were fabricated by following the same procedure as described in our previous publication.[43] Briefly, a droplet of gold nanoparticles was placed on a 10 nm thick gold-coated glass substrate. Then an OGMB was generated inside the droplet of nanoparticle solution. The convective flow induced by the OGMB helps to deposit gold nanoparticles on the gold-coated glass substrate to form ring-shaped nanogap-rich structures. It should be noted that the gold coating on the glass substrate is not a pre-requirement to generate the OGMB in this experiment. More discussion can be found in Fig. S6 and S7 in the ESI.† The two nanogap-rich structures (gold-nanosphere-structure and gold-nanoshell-structure) were fabricated under a laser intensity of 34 mW μm^{-2} and a laser exposure time was 2 minutes. A near-infrared continuous-wave laser of wavelength 1064 nm was used to generate the OGMB. The laser was focused on the substrate with a beam waist of around 0.7 μm. Therefore, the laser-based heating can deliver a high energy density to a small confined area for localized heating, which is challenging to achieve by using other methods such as thin-film resistive heaters.

SERS measurement

The SERS spectra of R6G and MG on the gold-nanosphere-structure and gold-nanoshell-structure were recorded with a Raman spectrometer (Renishaw inVia Reflex Micro-Raman) equipped with a near infrared diode laser source (maximum laser power: 300 mW and laser wavelength: 785 nm). R6G and MG were contained inside a sealed chamber that consists of a clean cover-glass on the top surface and a gold-coated glass substrate with the fabricated ring-shaped nanogap-rich structure as the bottom surface. The Raman exciting laser was carefully focused on R6G and MG molecules on the nanogap-rich structure with an objective lens (50×, NA = 0.75) to get the maximum Raman signal from the sample. Laser power on the sample was kept at 30 mW. Raman signals from all samples were collected for 10 second exposure time. It is worth noting that the heating laser and the Raman exciting laser can be the same laser to simplify the experimental setup.

Active sensing of analytes with an OGMB

During the active sensing of analytes, the size of the OGMB was around 175 ± 2 μm [Fig. S8(a)†] and the time duration of the OGMB was 2 minutes for all experimental data. The OGMB can be generated on the nanogap-rich structures at a laser intensity of 10 mW μm^{-2} for the active sensing of analytes, which is lower than the laser intensity of 34 mW μm^{-2} used for the fabrication of nanogap-rich structures. This reduction of the required laser intensity for the generation of an OGMB on nanogap-rich structures during the active sensing of analytes is a result of enhanced heating from gold nanoparticles, which has been studied in the literature.[52–54] The SERS signal increases with the increasing duration of the OGMB generation during the active sensing of analytes until it saturates at around 3.5 minutes of OGMB generation as shown in Fig. S8(b).†

Conflicts of interest

There are no conflicts of interest to declare.

Acknowledgements

The authors acknowledge the financial support from the University of Dayton STEM catalyst grant and Graduate Student Summer Fellowship provided by the Graduate Academic Affairs of the University of Dayton. This work was partially supported by the National Science Foundation under award number CMMI-1761132 for sharing equipment and materials.

References

1 P. R. Nair and M. A. Alam, *Appl. Phys. Lett.*, 2006, **88**, 233120.
2 P. E. Sheehan and L. J. Whitman, *Nano Lett.*, 2005, **5**, 803–807.
3 F. Karim, T. B. Smith and C. Zhao, *J. Nanophotonics*, 2017, **12**, 012504.
4 T. M. Squires, R. J. Messinger and S. R. Manalis, *Nat. Biotechnol.*, 2008, **26**, 417–426.
5 F. De Angelis, F. Gentile, F. Mecarini, G. Das, M. Moretti, P. Candeloro, M. L. Coluccio, G. Cojoc, A. Accardo, C. Liberale, R. P. Zaccaria, G. Perozziello, L. Tirinato, A. Toma, G. Cuda, R. Cingolani and E. Di Fabrizio, *Nat. Photonics*, 2011, **5**, 682–687.
6 P. R. Nair and M. A. Alam, *Nano Lett.*, 2008, **8**, 1281–1285.
7 G. McHale, N. J. Shirtcliffe and M. I. Newton, *Analyst*, 2004, **129**, 284.
8 L. Mahadevan and Y. Pomeau, *Phys. Fluids*, 1999, **11**, 2449–2453.
9 P. Aussillous and D. Quéré, *Nature*, 2001, **411**, 924–927.
10 G. McHale, S. Aqil, N. J. Shirtcliffe, M. I. Newton and H. Y. Erbil, *Langmuir*, 2005, **21**, 11053–11060.
11 S. Yang, X. Dai, B. B. Stogin and T.-S. Wong, *Proc. Natl. Acad. Sci. U. S. A.*, 2016, **113**, 268–273.
12 C. Escobedo, A. G. Brolo, R. Gordon and D. Sinton, *Nano Lett.*, 2012, **12**, 1592–1596.
13 F. Eftekhari, C. Escobedo, J. Ferreira, X. Duan, E. M. Girotto, A. G. Brolo, R. Gordon and D. Sinton, *Anal. Chem.*, 2009, **81**, 4308–4311.
14 D. S. Grubisha, R. J. Lipert, H.-Y. Park, J. Driskell and M. D. Porter, *Anal. Chem.*, 2003, **75**, 5936–5943.
15 A. Lesniewski, M. Los, M. Jonsson-Niedziółka, A. Krajewska, K. Szot, J. M. Los and J. Niedziolka-Jonsson, *Bioconjugate Chem.*, 2014, **25**, 644–648.
16 Y. Wang and E. C. Alocilja, *J. Biol. Eng.*, 2015, **9**, 16.
17 J. N. Anker, W. P. Hall, O. Lyandres, N. C. Shah, J. Zhao and R. P. Van Duyne, *Nat. Mater.*, 2008, **7**, 442–453.
18 S. Unser, I. Bruzas, J. He, L. Sagle, S. Unser, I. Bruzas, J. He and L. Sagle, *Sensors*, 2015, **15**, 15684–15716.
19 J. Garcia-Guirado, R. A. Rica, J. Ortega, J. Medina, V. Sanz, E. Ruiz-Reina and R. Quidant, *ACS Photonics*, 2018, **5**, 3673–3679.

20 D. Liu, F. Zhou, C. Li, T. Zhang, H. Zhang, W. Cai and Y. Li, *Angew. Chem., Int. Ed.*, 2015, **54**, 9596–9600.
21 D. Liu, C. Li, F. Zhou, T. Zhang, H. Zhang, X. Li, G. Duan, W. Cai and Y. Li, *Sci. Rep.*, 2015, **5**, 7686.
22 D. Liu, C. Li, F. Zhou, T. Zhang, G. Liu, W. Cai and Y. Li, *Adv. Mater. Interfaces*, 2017, **4**, 1600976.
23 S. Tian, O. Neumann, M. J. McClain, X. Yang, L. Zhou, C. Zhang, P. Nordlander and N. J. Halas, *Nano Lett.*, 2017, **17**, 5071–5077.
24 S. Yang, D. Slotcavage, J. D. Mai, F. Guo, S. Li, Y. Zhao, Y. Lei, C. E. Cameron and T. J. Huang, *J. Mater. Chem. C*, 2014, **2**, 8350–8356.
25 Y. Xie, S. Yang, Z. Mao, P. Li, C. Zhao, Z. Cohick, P.-H. Huang and T. J. Huang, *ACS Nano*, 2014, **8**, 12175–12184.
26 B. Kiraly, S. Yang and T. J. Huang, *Nanotechnology*, 2013, **24**, 245704.
27 X. Chen, N. C. Lindquist, D. J. Klemme, P. Nagpal, D. J. Norris and S.-H. Oh, *Nano Lett.*, 2016, **16**, 7849–7856.
28 B. B. Rajeeva, Z. Wu, A. Briggs, P. V. Acharya, S. B. Walker, X. Peng, V. Bahadur, S. R. Bank and Y. Zheng, *Adv. Opt. Mater.*, 2018, **6**, 1701213.
29 Y. Xie, C. Zhao, Y. Zhao, S. Li, J. Rufo, S. Yang, F. Guo and T. J. Huang, *Lab Chip*, 2013, **13**, 1772.
30 C. Zhao, Y. Xie, Z. Mao, Y. Zhao, J. Rufo, S. Yang, F. Guo, J. D. Mai and T. J. Huang, *Lab Chip*, 2014, **14**, 384–391.
31 Q. Fan, W. Hu and A. T. Ohta, *Lab Chip*, 2014, **14**, 1572–1578.
32 Q. Fan, W. Hu and A. T. Ohta, *Lab Chip*, 2015, **15**, 581–588.
33 Y. Xie and C. Zhao, *Nanoscale*, 2017, **9**, 6622–6631.
34 K. Setoura, S. Ito and H. Miyasaka, *Nanoscale*, 2017, **9**, 719–730.
35 C. Zhao, Y. Liu, Y. Zhao, N. Fang and T. Jun Huang, *Nat. Commun.*, 2013, **4**, 2305.
36 F. Meng, W. Hao, S. Yu, R. Feng, Y. Liu, F. Yu, P. Tao, W. Shang, J. Wu, C. Song and T. Deng, *J. Am. Chem. Soc.*, 2017, **139**, 12362–12365.
37 Y. Zheng, H. Liu, Y. Wang, C. Zhu, S. Wang, J. Cao and S. Zhu, *Lab Chip*, 2011, **11**, 3816.
38 L. Lin, X. Peng, Z. Mao, W. Li, M. N. Yogeesh, B. B. Rajeeva, E. P. Perillo, A. K. Dunn, D. Akinwande and Y. Zheng, *Nano Lett.*, 2016, **16**, 701–708.
39 S. Fujii, K. Kanaizuka, S. Toyabe, K. Kobayashi, E. Muneyuki and M. Haga, *Langmuir*, 2011, **27**, 8605–8610.
40 B. Bangalore Rajeeva, L. Lin, E. P. Perillo, X. Peng, W. W. Yu, A. K. Dunn and Y. Zheng, *ACS Appl. Mater. Interfaces*, 2017, **9**, 16725–16733.
41 K. Zhang, A. Jian, X. Zhang, Y. Wang, Z. Li and H. Tam, *Lab Chip*, 2011, **11**, 1389.
42 F. Tantussi, G. C. Messina, R. Capozza, M. Dipalo, L. Lovato and F. De Angelis, *ACS Nano*, 2018, **12**, 4116–4122.
43 F. Karim, E. S. Vasquez and C. Zhao, *Opt. Lett.*, 2018, **43**, 334.
44 S. A. Maier, *Plasmonics: Fundamentals and Applications*, Springer US, New York, NY, 2007, pp. 5–19.
45 H. A. Atwater, *Sci. Am.*, 2007, **296**, 56–62.
46 A. Polman, *Science*, 2008, **322**, 868–869.
47 C. Wu, E. Chen and J. Wei, *Colloids Surf., A*, 2016, **506**, 450–456.
48 F. Tian, F. Bonnier, A. Casey, A. E. Shanahan and H. J. Byrne, *Anal. Methods*, 2014, **6**, 9116–9123.
49 S. Y. Ding, E. M. You, Z.-Q. Tian and M. Moskovits, *Chem. Soc. Rev.*, 2017, **46**, 4042–4076.
50 A. Merlen, F. Lagugné-Labarthet and E. Harté, *J. Phys. Chem. C*, 2010, **114**, 12878–12884.
51 Y. Mo, J. Lei, X. Li and P. Wachter, *Solid State Commun.*, 1988, **66**, 127–131.
52 G. Baffou, J. Polleux, H. Rigneault and S. Monneret, *J. Phys. Chem. C*, 2014, **118**, 4890–4898.
53 K. Setoura, S. Ito and H. Miyasaka, *Nanoscale*, 2017, **9**, 719–730.
54 J. Chikazawa, T. Uwada, A. Furube and S. Hashimoto, *J. Phys. Chem. C*, 2019, **123**, 4512–4522.